3046–3055 *Nucleic Acids Research, 2015, Vol. 43, No. 6* *Published online 09 March 2015*
doi: 10.1093/nar/gkv098

Dissecting the behavior and function of MBD3 in DNA methylation homeostasis by single-molecule spectroscopy and microscopy

Yi Cui[1,2] and Joseph Irudayaraj[1,2,*]

[1]Department of Agricultural and Biological Engineering, 225 S. University Street, Purdue University, West Lafayette, IN 47907, USA and [2]Bindley Bioscience Center, 1203 W. State Street, Purdue University, West Lafayette, IN 47907, USA

Received April 24, 2014; Revised January 12, 2015; Accepted January 29, 2015

ABSTRACT

The detailed mechanism for DNA methylation homeostasis relies on an intricate regulatory network with a possible contribution from methyl-CpG-binding domain protein 3 (MBD3). In this study we examine the single-molecule behavior of MBD3 and its functional implication in balancing the activity of DNA methyltransferases (DNMTs). Besides a localization tendency to DNA demethylating sites, MBD3 experiences a concurrent transcription with DNMTs in cell cycle. Fluorescence lifetime correlation spectroscopy (FLCS) and photon counting histogram (PCH) were applied to characterize the chromatin binding kinetics and stoichiometry of MBD3 in different cell phases. In the G1-phase, MBD3, in the context of the Mi-2/NuRD (nucleosome remodeling deacetylase) complex, could adopt a salt-dependent homodimeric association with its target epigenomic loci. Along with cell cycle progression, utilizing fluorescence lifetime imaging microscopy-based Förster resonance energy transfer (FLIM-FRET) we revealed that a proportion of MBD3 and MBD2 would co-localize with DNMT1 during DNA maintenance methylation, providing a proofreading and protective mechanism against a possible excessive methylation by DNMT1. In accordance with our hypothesis, insufficient MBD3 induced by small interfering RNA (siRNA) was found to result in a global DNA hypermethylation as well as increased methylation in the promoter CpG islands (CGIs) of a number of cell cycle related genes.

INTRODUCTION

As a predominant epigenetic mechanism, DNA methylation that occurs at the 5-carbon of the pyrimidine ring in cytosine, substantially dictates the chromatin conformation and genetic activity. Conserved along proliferation, edited during differentiation and transgressed in pathogenesis, the patterns of genome-wide DNA methylation hold the key to cell fate and therefore ought to be maintained in a dynamic homeostasis (1). DNA methyltransferases (DNMTs), mainly including DNMT1 and DNMT3A/3B, are responsible for adding a methyl-group to the genomic sites, especially to CpG dinucleotides. However, the classical view to arbitrarily categorize those enzymes as maintenance DNMTs and *de novo* DNMTs appears to be challenged by cumulative evidence that expounds on the similarities of their function (2–5), which in turn necessitates revisiting the existing understanding on DNA methylation maintenance and homeostasis (6,7). Over the past decade it has been recognized that DNA maintenance methylation rarely follows a rigorous CpG-by-CpG fidelity, but adopts a stochastic model in which the twin forces of methylases and demethylases contend in an equilibrium, based on which the average methylation density of a specific DNA region can be well conserved (8). Ten-eleven-translocation proteins (TETs) were recently found to be a group of dioxygenases that enable the active DNA demethylation in mammalian cells, but they primarily function in early embryogenesis and some pathological malignancies to regulate gene expression (9). In the light of this, it is of great interest to resolve the question as to whether other balancing forces/machineries exist in cells to prevent a possible excessive methylation by DNMTs for DNA methylation homeostasis.

Methyl-CpG-binding domain protein 3 (MBD3) belongs to a family of nuclear proteins in close relation to DNA methylation, but exhibits elusive epigenomic association and functional identity (10–13). Although more than 70% of the MBD3 protein sequence is identical to MBD2, a number of researches utilizing *in vitro* binding assays or ChIP-seq have suggested that MBD3 might not be a *bona fide* binding protein for 5-methylcytosine (5mC), partially due to the K30H/Y34F mutations in its sequence (14–19). On the contrary, as a constitutive component of the

*To whom correspondence should be addressed. Tel: +1 765 404 0499; Email: josephi@purdue.edu

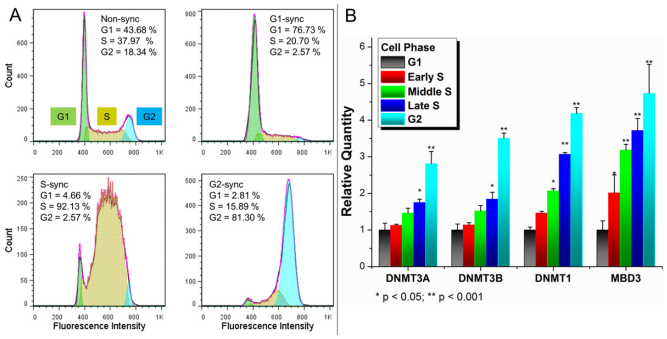

Figure 1. MBD3 transcription is concurrent with DNMTs during cell cycle progression. (**A**) Sequential cell synchronization was validated with flow cytometry followed by (**B**) quantitative RT-PCR for MBD3 and DNMTs. Relative quantity of each gene is normalized to the transcriptional level in the G1-phase and presented as the mean with standard deviation ($n = 4$). Student's *t*-test was used to determine the statistical significance.

Mi-2/NuRD complex, MBD3 has been found to preferentially localize at CpG-rich promoters and enhancers of active genes where DNA is poised for dynamic turnover of its methylation state (20–22). Nevertheless, an interesting commonality for MBD2 and MBD3 is that both possess the ability to induce DNA demethylation (23–26). Intriguingly, a proportion of MBD3, MBD2 and DNMT1 could co-appear in the DNA replication loci and bind to hemimethylated DNA (27), which inspired us to decipher the underlying implication of such a seemingly paradoxical cooperation.

Conventional approaches in biology research mostly rely on ensemble and end-point measurements from population of cells, thus overlooking the real-time heterogeneity and nano-scale kinetics of biomolecules. Single-molecule explorations open a unique window to inspect biological activities with unprecedented sensitivity and accuracy (28). In our previous work, we have demonstrated the potential of single-molecule techniques in uncovering some of the molecular dynamics and interactions involved in epigenetic regulation (29,30). Using fluorescence correlation spectroscopy (FCS) we have shown that the diffusion characteristics of MBD3 can be quantitatively correlated with active DNA demethylation events (31). In this study we incorporate a set of single-molecule fluorescence tools to dissect the behavioral dynamics of MBD3 in DNA methylation homeostasis from a cell cycle perspective. The rationale for our key hypothesis relating to the MBD3–MBD2–DNMT1 co-operation lies in the *in vivo* demethylating potential of MBD3 and MBD2 to buffer the activity of DNMT1 during cell cycle progression, to complement the epigenetic inheritance of loci-specific methylation density. Further, considering the significant size-disparity between the large DNMT1 protein (~10-15 nm) and methylated cytosine (~0.3 nm), the co-operation between DNMT1 and methyl-CpG-binding domain protein (MBD) can also increase the recognition sensitivity of DNMT1 to hemimethylation sites. In order to illustrate the proposed behavior in single intact cells, we focused on elucidating the biophysical characteristics of MBD3—intracellular dynamics, chromatin association, binding stoichiometry and molecular interactions using appropriate methods.

Quantitative single-molecule characterization provides us with tremendous opportunities to sense intracellular components. Enabled by recording of the fluorescence fluctuation owing to the molecular diffusion in a sub-femtoliter detection volume, FCS can provide a robust measure of dynamics at the microsecond level, from which subtle changes in biomolecular dynamics and association can be inferred (32–34). In this study, we applied fluorescence lifetime correlation spectroscopy (FLCS), an elegant derivative of FCS (35,36), to extract the real-time diffusion characteristics of MBD3 in different cell phases and found that MBD3 might have distinct DNA binding behaviors in the G1-phase and the G2-phase. Further, we analyzed the *in vivo* binding stoichiometry of MBD3 with photon counting histogram (PCH) and validated the salt-dependent 'two-site sequential binding' mode in the G1-phase nucleus. In the G2-phase, the co-localization of MBD3, MBD2 and DNMT1 was verified by FLIM-FRET, although the exact coupling mechanism for this co-operation requires further research. Upon siRNA mediated MBD3 knockdown, a global DNA hypermethylation and the significant increase in the methylation level of a number of promoter CGIs of cell cycle related genes were noted, which in turn could disrupt the normal cell cycle progression. Altogether, our study constitutes a pioneer effort to revise the model of DNA methylation homeostasis, which paves the way for future research to better interpret the epigenetic DNA methylome.

MATERIALS AND METHODS

Cell culture and cell cycle synchronization

HeLa cells were regularly cultured in DMEM/F-12 medium supplemented with 10% fetal bovine serum, 100 IU/ml penicillin and 100 μg/ml streptomycin in a humidified incubator supplemented with 5% CO_2 at 37°C. Synchronizing cells to different phases referred to established protocols (37–39). Generally, G1-phase enriched cells were obtained by treating cells with 400 μM L-mimosine (Sigma) for 20–24 h. To achieve a maximum S-phase population, cells were blocked with 2 mM thymidine (Sigma) for 20 h and released in fresh medium for 10 h, followed by 20 h of blocking with thymidine and finally culturing in fresh medium for another 4 h. Cultures containing G2-phase arrested cells were obtained by incubating with fresh medium containing 0.1 μg/ml KaryoMAX® Colcemid (Life Technologies) for 6 h after two rounds of thymidine blocking. Flow cytometry was used to assess cell cycle distribution. Cells were fixed with 70% ethanol and then stained with 20 μg/ml propidium iodide (PI) solution containing 0.1% Triton X-100 and 200 μg/ml RNase A, referring to standard protocol (40). Cell cycle distribution, through quantifying the PI fluorescence intensity, was determined in a FC500 MPL system (Beckman Coulter). At least 15 000 cells were collected for each condition and the generated cell cycle histograms were analyzed with Watson pragmatic model in Flowjo software package.

Quantitative RT-PCR

RNA extraction was conducted with RNeasy Mini Kit (Qiagen) followed by reverse transcription with iScript™ cDNA Synthesis Kit (Bio-Rad), according to the manufacturers' instructions, respectively. Before cDNA synthesis, genomic DNA was removed by treatment with DNase I. Polymerase chain reaction (PCR) amplification was performed in a StepOnePlus™ system (Applied Biosystems) with SYBR® Green PCR Master Mix (Life Technologies). The $\Delta\Delta Ct$ method was used to normalize all the transcription level to the internal control gene GAPDH. PCR primers for GAPDH, DNMT1, DNMT3A and DNMT3B were designed and optimized within Primer-BLAST online tools (http://www.ncbi.nlm.nih.gov/tools/primer-blast/). The PCR primers used in this study are listed in Supplementary Table S1.

Plasmid and siRNA transfection

Plasmid transfection was accomplished using Lipofectamine® LTX & Plus Reagent Kit (Life Technologies) according to the manufacturer's instruction with minor modifications. The expression vector of nucleus-green fluorescent protein (GFP) (Figure 3C, inset) was purchased from Life Technologies. Cells were seeded on sterilized No. 1 coverslips (VWR International) in a 12-well plate with 2 ml fresh medium. After reaching 70% confluence the medium was replaced with antibiotics-free, low-serum medium for another 12 h. Then 100 ng plasmid DNA, 2.5 μl LTX reagent and 0.1 μl Plus reagent were mixed into Opti-MEM® reduced-serum medium for each well. Transfection lasted for 24 h prior to live cell FLCS and PCH measurements. MBD3 siRNA, scrambled siRNA and transfection reagents for knockdown experiments were obtained from Santa Cruz Biotechnology. A total of 50 pmol siRNA was used for a 35 mm culture dish when cells reached 70% confluence according to the manufacturer's suggestion. Transfection lasted for 24 h followed by sub-culturing with normal fresh medium for another 72 h.

Single-molecule fluorescence system

Confocal fluorescence imaging, FLCS, PCH and FLIM-FRET experiments were performed with a Microtime200 scanning confocal time-resolved microscope system (Picoquant GmbH) (Supplementary Figure S1); A 465 nm picosecond pulsed laser was used to excite the GFP tag and Alexa488 labeled antibodies. Cy3 was excited by a 532 nm laser for *in vitro* PCH calibration. The excitation beam was delivered to the sample stage through an apochromatic water immersion objective (60×, N.A. = 1.2) and the fluorescence was collected by the same objective, after which the emission was separated by a dual band dichroic (z467/638rpc for blue laser, 49004 DCXR for green laser, Chroma). A 50 μm pinhole was employed to block the off-focus photons and the final signal was additionally filtered by a band-pass filter (520 ± 20 nm for green emission, 610 ± 30 nm for red emission, Chroma) before reaching the single photon avalanche photodiode detectors (SPAD) (SPCM-AQR, PerkinElmer Inc.). Fluorescence information was recorded using the TCSPC (time-correlated single photon counting) module in the time-tagged time-resolved (TTTR) mode (TimeHarp200). Raw fluorescence images and autocorrelation data were first analyzed and then exported with the SymPhoTime software package (PicoQuant GmbH) for further processing. For detailed mathematical fitting and analysis procedure, please refer to the Supplementary Methods.

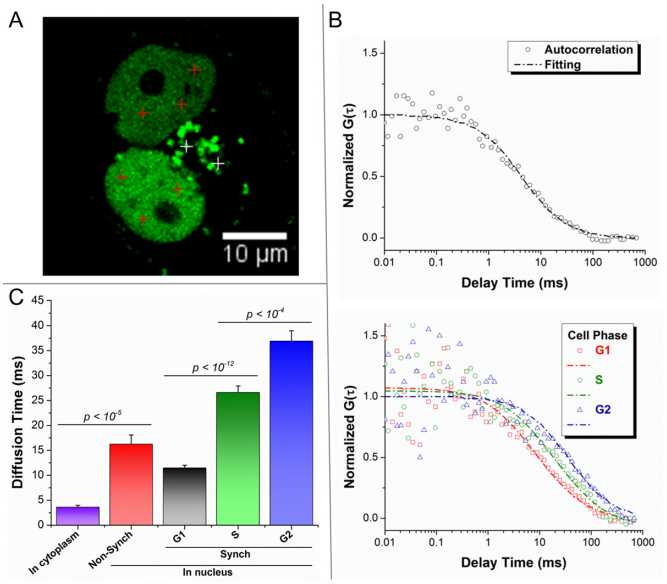

Figure 2. Restriction in the dynamics of nulcear MBD3 increases during cell cycle progression. (**A**) Illustration of FLCS data collection within different compartments (red cross for nucleus, white cross for cytoplasm) is shown. 2–3 measurement points were randomly chosen from each compartments. (**B**) Fitting autocorrelation curvers in FLCS: for cytoplamic MBD3-GFP (upper panel) a single-component 3D free diffusion model was used, while for nuclear MBD3-GFP (lower panel) an anomalous diffusion model was applied. (**C**) The MBD3-GFP diffusion times under different circumstances were obtained. Each group was summarized based on data from more than 15 cells (mean + standard error of the mean, $n > 30$). The 'unbound' measurements were mostly obtained from the free MBD3-GFP in cytoplasm.

Antibody labeling and immunofluorescence

In FLIM-FRET experiments, in order to minimize the overall size of antigen-antibody complex, primary antibodies (anti-MBD1/MBD2/MBD3/MTA2-IgG, Abcam; anti-DNMT1-IgG, Novus Biologicals; anti-5-Hydroxymethylcytosine (5hmC)/5-Formylcytosine (5fC)/5-Carboxylcytosine (5caC)-IgG, Active Motif) were directly labeled with fluorescent FRET-pair by APEX™ Antibody Labeling Kits (Life Technologies): MBD3 with Alexa488 (donor); MBD1, MBD2, MTA2, DNMT1, 5hmC, 5fC and 5caC with Alexa555 (acceptor). For immunofluorescence staining, cells were fixed with 4% paraformaldehyde for 15 min at 4°C and rinsed with 1× phosphate buffered saline (PBS) buffer. Cell membrane was permeabilized by 0.4% Triton X-100 (Sigma) for 30 min and rinsed with clean PBS for 15 min. After HCl treatment (optional for DNA denaturation), cells were then blocked with PBS containing 5% goat serum and 0.3% Triton X-100 for 1 h. Labeled primary antibodies were diluted 100× (~5 nM) in PBS containing 1% BSA and 0.3%

Triton X-100 to incubate with cells overnight at 4°C. In the next day cells were rinsed 3× with PBS prior to FLIM imaging. For semi-quantification of MBD3 and H3K27ac by immunofluorescence, standard staining procedure was performed: 1:1000 dilution of the primary antibody (e.g. anti-H3K27ac-IgG, Active Motif) and secondary antibody (Alexa Fluor®488 F(ab')$_2$ fragment of Goat anti-Rabbit IgG (Life Technologies)) were sequentially applied and incubated overnight and 1 h prior to confocal imaging.

Immunoassay for global DNA methylation and quantitative PCR array for promoter CGIs methylation of cell cycle related genes

DNA from control and siRNA treated cells was extracted and purified with DNeasy Blood & Tissue Kit (Qiagen), according to the manufacturer's instruction. Global DNA methylation level was determined by MethylFlash™ Methylated DNA Quantification Kit (Epigentek). Briefly, 100 ng of DNA was deposited to the bottom of the assay well followed by incubation with capture antibody and detection antibody, sequentially. The final colorimetric signal was normalized to the standard input DNA to estimate the overall methylation percentage. Twenty-two key genes involved in cell cycle progression were assessed for their promoter CGIs methylation levels using EpiTect® Methyl II Signature PCR Array (Qiagen). The general working mechanism for this array is achieved by treating input DNA with methylation-sensitive endonuclease (unmethylated CGIs will be digested) or methylation-dependent endonuclease (methylated CGIs will be digested). Upon PCR amplification with specific primers targeting the characterized promoter CGIs of each gene, the percentage of methylated promoters in the corresponding input sample can be determined.

RESULTS

Localization preference and cell cycle-dependent transcription of MBD3

We first evaluated the localization preference of endogenous MBD3 in HeLa cells using FLIM-FRET, to explore its possible relation with 5mC derivatives. The anti-MBD3-IgG labeled with Alexa488 served as the FRET donor, while the anti-5hmC/5fC/5caC-IgG labeled with Alexa555 served as the FRET acceptor. Before FRET experiments, we optimized the DNA denaturation procedure for 5hmC/5fC/5caC staining using hydrogen chloride (HCl), considering the negative impact of acid on fluorescence lifetime and antibody performance. We determined that treating cells with 1 N HCl at 37°C for 30 min is compatible with FLIM imaging and antibody specificity (Supplementary Figure S2A). From the FLIM-FRET exploration, a relatively low co-localization between MBD3 and 5hmC was suggested from the calculation of FRET efficiency. In comparison, MBD3 exhibited a prominent co-localization preference to 5fC and 5caC (Supplementary Figure S2), which is in agreement with the most recent findings (17,18). These results provide partial support to the *in vivo* demethylating potential of MBD3 due to its spatial co-existence with the oxidized derivatives of 5mC and

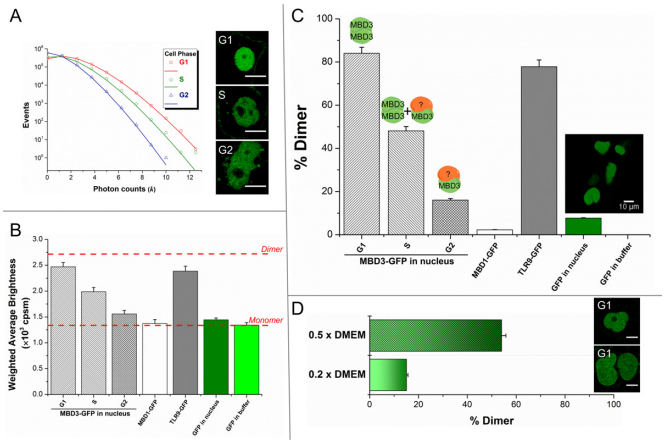

Figure 3. Analysis of single-molecule brightness by PCH implicates a transition of MBD3 binding stoichiometry. (**A**) Photon counting histograms from nuclear MBD3-GFP in different cell phases are presented along with corresponding images. (**B**) Weighted average brightness of different GFP tagged constructs was obtained, with pure GFP as the brightness standard, TLR9-GFP as the dimer control and MBD1-GFP as the monomer control. (**C**) Dimer percentage for each protein was calculated based on the brightness of pure GFP in buffer. (**D**) Hypotonic medium disrupted the dimer formation of MBD3-GFP in the G1-phase nucleus. Scale bar: 10 μm.

5hmC. Since no direct *in vitro* enzymatic activity was characterized for pure MBD3, the nearby DNA demethylation could possibly be a consequence of the MBD3 mediated recruitment of TET proteins (15) or other unknown mechanisms (e.g. via steric hindrance to block the DNMTs functionality). Next, cells synchronized to be in different phases with appropriate treatments were obtained and validated by flow cytometry (Figure 1A). Upon synchronization, transcripts of MBD3 and all three DNMTs were quantified with quantitative RT-PCR. Our experiments show an increase of the DNMTs at the start of the S-phase to maintain a high abundance till the G2-phase for cells to fully complete the maintenance methylation on hemi-methylated DNA (Figure 1B), which is consistent with the previous research exploring the cell cycle-dependent expression of DNMTs (41). It was initially perceived that the transcription of DNMTs should peak during the S-phase rather than the G2-phase. However, the two critical points to bear in mind are that the DNA maintenance methylation has been characterized as a delayed event compared to DNA replication and in cancerous or transformed cells the regulation of the expression of DNMTs could further be delayed due to rapid cell proliferation (2,41,42). Interestingly, similar to DNMTs, the transcription of MBD3 also experiences a cell cycle-dependent enrichment. This concurrent change provides preliminary evidence for an underlying connection, at the transcriptional level, between MBD3 and DNMTs to support their contention and co-operation in DNA methylation homeostasis.

The mobility of MBD3 is increasingly constrained during the G1–S–G2 transition

Taking advantage of the statistical filtering function in FLCS, the noise in the autocorrelation fluctuation due to

the detector (e.g. thermal noise and afterpulses) and other signal components (e.g. elastic scattering and Raman signal) that occur at the millisecond or lower timescale can be greatly eliminated (Supplementary Figure S3)(36,43). For live cell FLCS measurement, different from in standard lipofectamine transfection, we used a much less plasmid DNA (10-fold lower) to decrease the expression of redundant MBD3-GFP in cell nucleus. Upon optimization, ∼60% tranfection efficiency and an average concentration of 80 nM intra-nucleus MBD-GFP were achieved for the following single-molecule experiments. Hence, the natural diffusion dynamics of MBD3-GFP can be well extracted from a single-component anomalous diffusion model. Data collection points for FLCS measurement were randomly chosen from more than 15 cells as represented in Figure 2A. Generally, using 60 s as the integration window to generate autocorrelation functions, the diffusion rate of MBD3-GFP in the cytoplasm (unbound) was found to be much faster (a diffusion time of 3.6 ± 0.4 ms) than that in the nucleus (a diffusion time of 16.2 ± 1.9 ms) of non-synchronized cells, which is consistent with our previous study (Figure 2B and C)(31). The significantly slower diffusion of MBD3-GFP in the nucleus could be attributed to two mechanisms: its integration into the Mi-2/NuRD complex and the subsequent association with the targeting chromatin site. To validate the integration of exogenous MBD3-GFP into the Mi-2/NuRD, we performed FLIM-FRET experiments between MBD3-GFP and the endogenous MTA2 protein (a key component of the Mi-2/NuRD) labeled with Alexa555. A gradual reduction in the GFP fluorescence lifetime after transfection was observed (Supplementary Figure S4), indicating the association of MBD3-GFP with the Mi-2/NuRD. Then the cell cycle-dependent dynamics of MBD3-GFP was probed. Upon comparison with the MBD3-GFP in the cells synchronized in the G1-phase, the MBD3-GFP in the S-phase and the G2-phase exhibited drastically slower diffusion rates: diffusion times noted are 11.5 ± 0.6 ms (G1), 26.6 ± 1.3 ms (S) and 36.9 ± 2.1 ms (G2), respectively (Figure 2C). Moreover, an incremental adjustment in the 'degree of anomalous behavior' ('α' in Supplementary Equation 3) was required to fit the autocorrelation curves along with the G1–S–G2 transition, reflecting a strengthened restriction in the mobility of MBD3-GFP. Considering the fact that molecular diffuison is negatively proportional to the hydrodynamic radius (Stokes–Einstein relation), our obtained FLCS results suggest that, starting from the S-phase, the MBD3/NuRD complex may further associate with or recruit other large biomolecules to the relevant genomic sites, giving rise to an enhanced DNA binding affinity.

MBD3/NuRD experiences a transition of binding stoichiometry in the S-phase

PCH can provide information on homogeneous stoichiometry based on the average brightness on a per molecule basis and well established controls. The weighted average brightness of nuclear MBD-GFP was then evaluated in different cell phases by PCH, from which a gradual reduction of the measured GFP brightness was observed when cells progressed through G1–S–G2 phases (Figure 3A). To calibarate the GFP fluorescence-based molecular stoichiometry, we have carefully designed necessary controls: pure GFP in buffer and in cell nucleus, toll-like receptor 9-GFP (TLR9-GFP) and MBD1-GFP in live cells. We extracted and purified monomer GFP proteins to establish standards and the brightness was calculated to be 1341 ± 48 cpsm (counts per second per molecule) under a 2.5 μW excitation power (Figure 3B). Based on this value, we can deconvolve the obtained average bightness of GFP tagged fusion proteins into monomeric and dimeric components and a non-specific dimerization rate of ∼8% for pure GFP was also determined in living HeLa cells. We used a well characterized and standardized TLR9-GFP model as the dimer control from our previous study on defining the TLR9-GFP dimerization on its binding target in living cells (44). From PCH analysis, the percentage of dimers for TLR9-GFP and MBD1-GFP was found to be 78 and 2%, respectively. Results for MBD3-GFP indicate that its binding stoichiometry also experienced a cell cycle-dependent transition: the dimer percentage altered from 84% in the G1-phase, to 48% in the S-phase and eventually to 16% in the G2-phase (Figure 3C). In a recent *in vitro* study, MBD domain was shown to sequentially dimerize onto a single (methyl-)CpG site under physiological condition and this binding specificity is salt/cation-dependent (45). Therefore we proposed that a low salt environment should be sufficient to undermine the binding specificity of MBD3 and its *in situ* dimerization in living cells as well. By applying a hypotonic culture medium to G1-phase cells, indeed the dimer proportion of MBD3-GFP significantly decreased (Figure 3D). In our hypothesis, the following stoichiometric transition of MBD3 in the S-phase is facilitated by the co-operation among MBD3, MBD2 and DNMT1 to realize DNA maintenance methylation, which is also supported by our FLCS results: MBD3

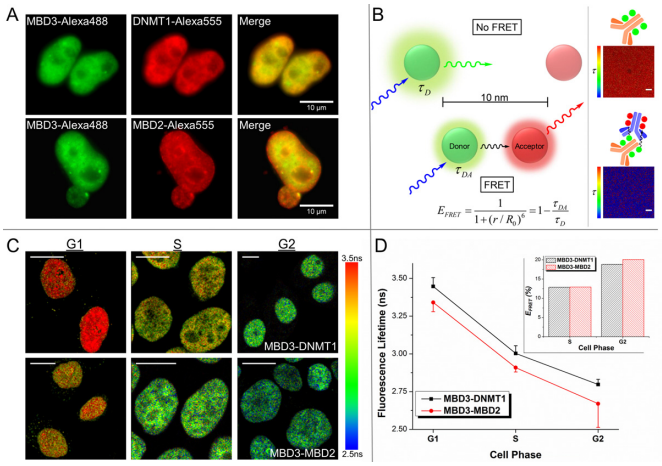

Figure 4. The MBD3–MBD2–DMNT1 complex in DNA maintenance methylation was assessed by FLIM-FRET. (**A**) Labeled primary antibodies were applied to target the protein pairs (MBD3–DNMT1, MBD3–MBD2). (**B**) A shortened fluorescence lifetime due to FRET is reflected by the blue-shift in FLIM images (an *in vitro* antibody-mediated FLIM-FRET is illustrated). (**C**) FLIM images of the Alexa488 labeled onto anti-MBD3-IgG were obtained in different cell phases, with DNMT1 or MBD2 directly labeled with Alexa555. Scale bar: 10 μm. (**D**) The ensemble-based fluorescence lifetimes are presented with mean and stand deviation ($n = 10$ images). FRET efficiencies were accordingly calculated (inset).

was shown to gradually reside into a larger complex (inferred from the slowed diffusion rate) and possess higher binding affinity with chromatin (inferred from the increased anomalous diffusion behavior) during cell cycle progression. These single-molecule observations from FLCS and PCH implicate that the difference in the internal molecular bonds of MBD3–DNA and MBD3–MBD2–DNMT1 may serve as the driving force to mechanistically advance the stoichiometric transition, for which the intracellular microenvironment (e.g. regional salt concentration) may be substantially involved.

MBD3, MBD2 and DNMT1 act in concert in DNA maintenance methylation

Although quite a few tools in conventional molecular biology such as co-immunoprecipitation, affinity electrophoresis, pull-down assay and yeast two-hybrid screening are available to evaluate biomolecular interactions, a challenge is to directly visualize *in situ* dynamic associations in the subcellular compartments. Nowadays fluorescence super-resolution microscopy is able to break the diffraction limit imposed by the conventional optics to achieve a 20–100 nm resolution for single cell imaging. However, the spatial scale (<10–20 nm) of most protein–protein and protein–DNA interactions is still beyond the 'super-resolution' scope. In this study we took advantage of the FRET mechanism as our biophysical ruler to probe the potential molecular interactions at the 10 nm level (Figure 4B, left panel). By directly labeling the primary antibodies against targets of interest with fluorescent FRET-pair (i.e. Alexa488 and Alexa555), dual-immunofluorescence staining was performed and the FRET signal was thus monitored via FLIM imaging in different cell phases (Figure 4A). As expected, a gradually occurring FRET reflected by the decrease in the lifetime of Alexa488 attached on anti-MBD3-IgG was noted in both combinations (MBD3–MBD2, MBD3–DNMT1) (Figure 4C). In FLIM images, longer lifetimes are represented by the red color whereas a blue-shift indicates a shorter lifetime as depicted by the scale bars (Figure 4B, right panel). In Figure 4C, the intense blue-shift in the MBD3-Alexa488 channel along with the G1–S–G2 progression clearly indicates a process that a growing portion of MBD3, MBD2 and DNMT1 can potentially assemble to form a larger complex. Statistically, in the G1-phase, MBD3-Alexa488 in the presence of MBD2-Alexa555 has a relatively shorter lifetime (3.34 ± 0.06 ns) than that in the presence of DNMT1-Alexa555 (3.45 ± 0.06 ns) (Figure 4D), implicating that some of the endogenous MBD3–MBD2 coexistence could be cell cycle-independent, which is supported by previous reports (11,27,46,47). In the control experiments, no such co-localization signal was observed between MBD3 and MBD1 (Supplementary Figure S6). Moreover, all these probed molecular interactions were validated with the MBD3-GFP-based co-immunoprecipitation (Supplementary Figure S7). Taken together, for the first time, the behavioral paradigm of the MBD3 interactome in DNA maintenance methylation was revealed by single-molecule tools within single cells (Figure 5).

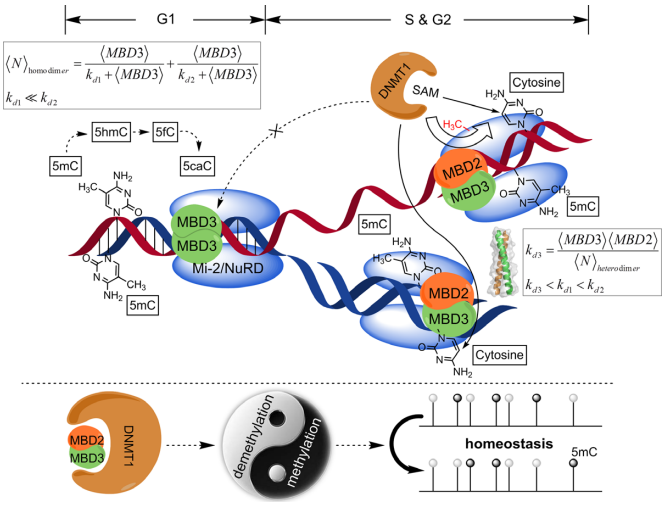

Figure 5. The dynamic characteristics of MBD3 in DNA methylation homeostasis. In the G1-phase, MBD3/NuRD adopts a 'two-site sequential binding mode' on its recognition CGIs and facilitates maintaining a hypomethylated state. k_{d1} and k_{d2} denote the two dissociation constants for the homodimeric binding. As the DNA starts to replicate, the newly synthesized hemi-methylated DNA intends to inherit the average methylation density from the parental template, conducted by DNMTs (mainly DNMT1). A proportion of MBD3 and MBD2 (a *bona fide* 5mC binding protein) would co-operate with DNMT1 herein to complement the accuracy of maintenance methylation. The demethylating potential of MBD3 and MBD2 provides a protective mechanism contributing to DNA methylation homeostasis in the S-G2 phases.

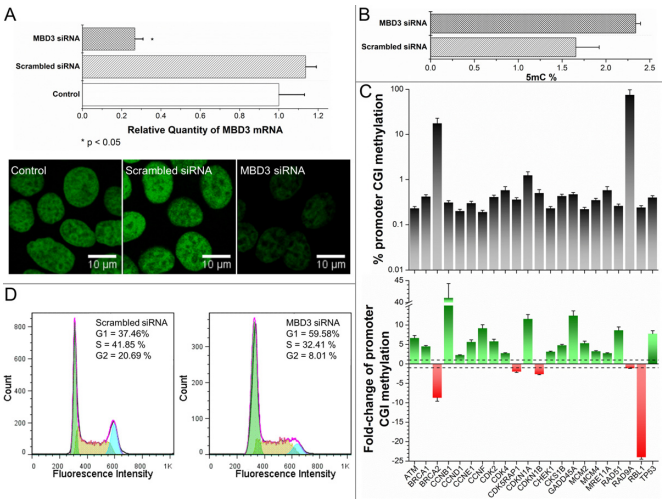

Figure 6. Disrupted DNA methylation homeostasis due to insufficient MBD3. (**A**) The siRNA knockdown effect was verified by quantitative RT-PCR and immunofluorescence. Upon MBD3 knockdown, (**B**) the global DNA methylation level was quantified with colorimetric immunoassay, (**C**) and the promoter CGIs methylation of 22 cell cycle related genes was quantified with PCR Array (presented as mean with standard deviation, $n = 3$). (**D**) Seventy-two hours after knockdown, the cell cycle distribution was analyzed by flow cytometry.

Insufficient MBD3 disrupts DNA methylation homeostasis

Following the single-molecule experiments, we assessed the possible impacts to DNA methylation upon suppressing the expression of MBD3, to support the functional involvement of MBD3 in DNA methylation homeostasis. We success-

fully inhibited the MBD3 transcription by ∼75% by introducing the specific siRNA targeting MBD3 mRNA (Figure 6A, upper bar chart), which subsequently resulted in a significant reduction of MBD3 proteins in HeLa cells (Figure 6A, lower panel). In agreement with our previous research that insufficient MBD3 would lead to the disorder and mis-assembly of Mi-2/NuRD (48), an aberrant accumulation of H3K27ac in MBD3 knockdown cells was observed (49)(Supplementary Figure S8). Given that MBD3 facilitates the maintenance of a hypomethylated state at its binding sites and participates in balancing DNA maintenance methylation, it was expected that the cells would experience a global hypermethylation upon MBD3 knockdown. Taking use of colorimetric quantitative immunoassay, the global level of DNA methylation in knockdown cells was found to increase from 1.66 to 2.34% compared to control cells after 72 h (Figure 6B). In parallel, we also evaluated the promoter CGIs methylation of 22 cell cycle involved genes since MBD3 has been discovered to modulate cell cycle progression through related genes (26,50). The promoter CGIs of the selected genes, except BRCA2 and RAD9A, were determined to be extensively hypomethylated or unmethylated in HeLa cells, consistent with the records in the ENCODE database and previous research (51). When the MBD3 level was suppressed, a ubiquitous elevation in the methylation of assessed CGIs was observed, though some changes were subtle due to a short knockdown period (Figure 6C). Furthermore, the effect of overexpressing MBD3 was assessed to support its *in vivo* demethylating potential in HeLa cells (Supplementary Figure S9). Considering the influence of MBD3 on the Mi-2/NuRD function and DNA methylation process, the normal cell cycle progression is subjected to dysfunction once MBD3 is deregulated. Thereafter we examined the cell cycle progression under the knockdown condition and found a larger population of cells arrested in the G1-phase, resembling the effect of directly impairing the Mi-2/NuRD or DNMTs (52–54). Overall, this set of experiments supports our proposed model derived from the biophysical characterization: the demethylating potential of MBD3 plays a critical role in sustaining DNA methylation homeostasis and cell physiology.

DISCUSSION

Achieving DNA methylation homeostasis necessitates the interplay of multiple molecules and mechanisms. For one single nucleosome covering about 200 bp of DNA (including linker), 3–10 CpG dinucleotides could statistically exist with an inheritable extent of methylation. In order to stably retain the average methylation level of a given DNA region across generations, a unified stochastic model recently developed was applied (7):

$$\frac{d\theta_{\mathrm{m}}^{i}}{dt} = r_{\mathrm{met}}^{i} \times (1-\theta_{\mathrm{m}}^{i}) - \left(\frac{1}{2}D\left(1-f_{\mathrm{main}}^{i}\right)+r_{\mathrm{demet}}^{i}\right)\times\theta_{\mathrm{m}}^{i} \quad (1)$$

Accordingly, the steady-state methylation level at a genomic locus ($\theta_{\mathrm{m}}^{i,ss}$) is practically attributed to multiple variables—the rate of cell division (D), the efficiency of maintenance methylation (f_{main}^{i}), the rate of demethylation (r_{demet}^{i}), the rate of *de novo* methylation (r_{met}^{i}), and can be expressed as:

$$\theta_{\mathrm{m}}^{i,ss} = \frac{r_{\mathrm{met}}^{i}}{\frac{1}{2}D\left(1-f_{\mathrm{main}}^{i}\right)+r_{\mathrm{demet}}^{i}+r_{\mathrm{met}}^{i}} \quad (2)$$

Derived from the above equation, the counteracting forces of demethylating and methylating were characterized by:

$$r_{\mathrm{demet}}^{i} = \frac{1-\theta_{\mathrm{m}}^{i,ss}}{\theta_{\mathrm{m}}^{i,ss}} \times r_{\mathrm{met}}^{i} + \frac{1}{2}D \times f_{\mathrm{main}}^{i} - \frac{1}{2}D \quad (3)$$

Upon incorporating the involvement (r^{i}) of the DNA methylation related proteins, we can roughly define that: $f_{\mathrm{main}}^{i} \propto r_{\mathrm{DNMT1}}^{i}$, $r_{\mathrm{met}}^{i} \propto r_{\mathrm{DNMT3A}}^{i} + r_{\mathrm{DNMT3B}}^{i}$, $r_{\mathrm{demet}}^{i} \propto r_{\mathrm{TETs}}^{i} + r_{\mathrm{MBD2/3}}^{i}$. In the G1-phase, MBD3 tends to anchor on active gene-loci and protect the hypomethylated state from DNMT3A/B invasion. In the S-G2 phases, DNMT1 as a major player, together with DNMT3A/B, participates in DNA maintenance methylation, whereas no experimental evidence has observed the direct involvement of TETs in this process. Without a real-time demethylating potential or proofreading mechanism, the delicate DNA methylome would become fairly vulnerable to non-equilibrium whenever DNMT1 overacts (e.g. $f_{\mathrm{main}}^{i} > 1$). In line with the previous research (13,26,27), our study reveals the dynamic behavior of MBD3 and its importance in DNA methylation homeostasis herein. When cells enter the cell cycle, a considerable portion of MBD3 and MBD2 would co-localize with DNMT1 to offer a favorable condition for the ongoing DNA maintenance methylation. In parallel, the concomitant Mi-2/NuRD positioning can assist the nucleosome remodeling and histone acetylation patterning during epigenetic inheritance. In the light of the uncovered dynamic behavior of MBD3, we reason that the occupancy sites for MBD3/NuRD would vary at different time points even within a single cell cycle, which might partially explain the divergent observations of genome-wide MBD3 distribution from previous studies (15,17,18).

The core region sequence among human MBD superfamily members for methyl-CpG recognition and binding is highly conserved (Supplementary Figure S10A). To date the already identified residues critical for MBD–DNA complex include VAL20, ARG22, LYS30, TYR34, ARG44 and SER45, in which the two arginine residues overwhelmingly determine the binding mechanism through a hydrogen bond and cation-π interaction-based 'stair motif' (Supplementary Figure S10B)(14,55,56). Although MBD3 is nearly identical to MeCP2 and MBD2 in the core region (Supplementary Figure S10C), the two crucial mutations (K30H and Y34F), located at the interface, biochemically only ensures its association specificity with CpG rather than exclusively with 5mC or 5hmC. Consistent with the recent discovery that MBD3 primarily localizes at active epigenetic loci, such as enhancers and promoters, our FLIM-FRET approach suggests an *in situ* spatial interaction between MBD3 and the 5mC-oxidized derivatives (i.e. 5hmC, 5fC

and 5caC which are difficult to be differentiated from cytosine in conventional DNA-sequencing methods), to support its potential in DNA demethylation and gene activation (17,18,20,22).

The binding stoichiometry between MBD and its targeting site was elusive and even controversial from different studies. Until very recently, a 'two-site sequential binding mode' has been proposed and biochemically validated (45). It demonstrated that, under physiological condition, the MBD-mediated DNA binding would adopt and tolerate the homodimeric association on a single CpG site but with distinct dissociation constants for each MBD, ranging from ∼80 nM to 5 μM. Moreover, a low salt concentration can significantly compromise the specificity for MBD to recognize CpG over random DNA sequences since monovalent cations are crucial to suppress the non-specific binding (45). This explains why the observed homodimeric state of MBD3/NuRD in the G1-phase got substantially reduced when a hypotonic medium was applied in our study. On the contrary, MBD1 was found to exist predominantly in a monomeric state. We speculate this stoichiometry is due to the preferable localization of MBD1 at the highly condensed heterochromatin where its potential dimerization could be impeded due to steric hindrance. One of our findings requiring future elucidation is on the MBD3/NuRD stoichiometric transition from the G1-phase to the G2-phase. According to our hypothesis, the co-existence of MBD2–MBD3–DNMT1 aids in achieving a homeostatic DNA maintenance methylation, while the detailed mechanism to form such multi-component machinery is challenging to resolve. MBD2 and DNMT1 have a theoretical basis to co-localize because of their ability to recognize hemi-methylated sites. For the recruitment of MBD3/NuRD, several possibilities might exist. One is through other epigenetic marks, such as histone modifications. MBD2, in the context of Mi-2/NuRD, can induce regional histone hypoacetylation which would subsequently attract MBD3/NuRD (11,13). Another is through the coiled-coil interaction. The key helix residues to form coiled-coil oligomer are highly conversed among MBD proteins across species, though a stable MBD2–MBD3 heterodimer was hard to detect by gel filtration analysis (57). However, considering the fact that the coiled-coil interaction is contingent with protein conformation and thus the surrounding physicochemical factors (58), we cannot rule out the possibility of a cell cycle-dependent *in vivo* coiled-coil MBD3–MBD2 interaction. In addition, since the p66α, a critical component of the Mi-2/NuRD, can firmly form heterodimer with either MBD2 or MBD3 (57,59), an indirect alternative to link MBD3 and MBD2 could be implied—in the context of a multimer bridged by p66α or other coiled-coil domain proteins. Notably, the dissociation constant for coiled-coil mediated interaction can reach the level of ∼10 nM, a much stronger affinity than the MBD–DNA binding, conducive to facilitate the disintegration of MBD3 from the original homodimers. The primary concern in this assumption is how the coiled-coil interaction gets inhibited in the G1-phase. Last, in the process of recruiting biomolecules to maintain DNA methylation, the potential contribution from the classical DNA replication related proteins, such as PCNA and UHRF1, should not be overlooked. Further effort can be placed in understanding the triggering mechanism for this stoichiometric transition and the detailed interactome.

In phenotypic analysis, MBD3 has been shown to play a deterministic role in embryogenesis, pluripotency, differentiation, reprograming and a variety of diseases, highlighting its functional importance (13,48,60–63). Disrupting the expression pattern of MBD3 unequivocally results in abnormal DNA methylation, but an in-depth exploration is lacking. Our study, combining single-molecule probing and biological validation, provides a new dimension to inspect the underlying mechanistic connection. We emphasize the biophysical properties of MBD3 and its *in vivo* demethylating potential as a pivotal balancing strength to merit DNA methylation homeostasis. This characteristic feature not only supports the basal expression of the occupied active gene-loci (e.g. cell cycle progression involved genes) but also constitutes a protective mechanism to buffer the possible overactivity of DNMTs.

SUPPLEMENTARY DATA

Supplementary Data are available at NAR Online.

ACKNOWLEDGEMENTS

We thank Dr Adrian Bird (University of Edinburgh, UK) for providing the MBD3-GFP and MBD1-GFP plasmids, Dr Jiji Chen (National Cancer Institute, USA) for the TLR9-GFP plasmid, Drs Amy C. Lossie and Chiao-Ling Lo (Purdue University, USA) for plasmid maintenance and purification. The insightful discussion with Dr Basudev Chowdhury (Purdue University, USA) greatly helped the content of this work.

FUNDING

W.M. Keck Foundation Grant; NSF [#1249315]; NIH-NCI Cancer Center Core [P30CA023168]. Fundingfor open access charge: NIH-NCI Cancer Center Core [P30CA023168]; NSF [#1249315]; W.M. Keck Foundation.
Conflict of interest statement. None declared.

REFERENCES

1. Jones,P.A. (2012) Functions of DNA methylation: islands, start sites, gene bodies and beyond. *Nat. Rev. Genet.*, **13**, 484–492.
2. Liang,G., Chan,M.F., Tomigahara,Y., Tsai,Y.C., Gonzales,F.A., Li,E., Laird,P.W. and Jones,P.A. (2002) Cooperativity between DNA methyltransferases in the maintenance methylation of repetitive elements. *Mol. Cell. Biol.*, **22**, 480–491.
3. Lorincz,M.C., Schubeler,D., Hutchinson,S.R., Dickerson,D.R. and Groudine,M. (2002) DNA methylation density influences the stability of an epigenetic imprint and Dnmt3a/b—independent de novo methylation. *Mol. Cell. Biol.*, **22**, 7572–7580.
4. Walton,E.L., Francastel,C. and Velasco,G. (2011) Maintenance of DNA methylation: Dnmt3b joins the dance. *Epigenetics*, **6**, 1373–1377.
5. Arand,J., Spieler,D., Karius,T., Branco,M.R., Meilinger,D., Meissner,A., Jenuwein,T., Xu,G., Leonhardt,H., Wolf,V. *et al.* (2012) In vivo control of CpG and non-CpG DNA methylation by DNA methyltransferases. *PLoS Genet.*, **8**, e1002750.
6. Jones,P.A. and Liang,G.N. (2009) OPINION Rethinking how DNA methylation patterns are maintained. *Nat. Rev. Genet.*, **10**, 805–811.

7. Jeltsch,A. and Jurkowska,R.Z. (2014) New concepts in DNA methylation. *Trends Biochem. Sci.*, **39**, 310–318.
8. Riggs,A.D. and Xiong,Z.G. (2004) Methylation and epigenetic fidelity. *Proc. Natl. Acad. Sci. U.S.A.*, **101**, 4–5.
9. Pastor,W.A., Aravind,L. and Rao,A. (2013) TETonic shift: biological roles of TET proteins in DNA demethylation and transcription. *Nat. Rev. Mol. Cell Biol.*, **14**, 341–356.
10. Hendrich,B. and Bird,A. (1998) Identification and characterization of a family of mammalian methyl-CpG binding proteins. *Mol. Cell. Biol.*, **18**, 6538–6547.
11. Zhang,Y., Ng,H.H., Erdjument-Bromage,H., Tempst,P., Bird,A. and Reinberg,D. (1999) Analysis of the NuRD subunits reveals a histone deacetylase core complex and a connection with DNA methylation. *Genes Dev.*, **13**, 1924–1935.
12. Wade,P.A., Gegonne,A., Jones,P.L., Ballestar,E., Aubry,F. and Wolffe,A.P. (1999) Mi-2 complex couples DNA methylation to chromatin remodelling and histone deacetylation. *Nat. Genet.*, **23**, 62–66.
13. Hendrich,B., Guy,J., Ramsahoye,B., Wilson,V.A. and Bird,A. (2001) Closely related proteins MBD2 and MBD3 play distinctive but interacting roles in mouse development. *Genes Dev.*, **15**, 710–723.
14. Saito,M. and Ishikawa,F. (2002) The mCpG-binding domain of human MBD3 does not bind to mCpG but interacts with NuRD/Mi2 components HDAC1 and MTA2. *J. Biol. Chem.*, **277**, 35434–35439.
15. Yildirim,O., Li,R., Hung,J.H., Chen,P.B., Dong,X., Ee,L.S., Weng,Z., Rando,O.J. and Fazzio,T.G. (2011) Mbd3/NURD complex regulates expression of 5-hydroxymethylcytosine marked genes in embryonic stem cells. *Cell*, **147**, 1498–1510.
16. Hashimoto,H., Liu,Y., Upadhyay,A.K., Chang,Y., Howerton,S.B., Vertino,P.M., Zhang,X. and Cheng,X. (2012) Recognition and potential mechanisms for replication and erasure of cytosine hydroxymethylation. *Nucleic Acids Res.*, **40**, 4841–4849.
17. Spruijt,C.G., Gnerlich,F., Smits,A.H., Pfaffeneder,T., Jansen,P.W., Bauer,C., Munzel,M., Wagner,M., Muller,M., Khan,F. *et al.* (2013) Dynamic readers for 5-(hydroxy)methylcytosine and its oxidized derivatives. *Cell*, **152**, 1146–1159.
18. Iurlaro,M., Ficz,G., Oxley,D., Raiber,E.A., Bachman,M., Booth,M.J., Andrews,S., Balasubramanian,S. and Reik,W. (2013) A screen for hydroxymethylcytosine and formylcytosine binding proteins suggests functions in transcription and chromatin regulation. *Genome Biol.*, **14**, R119.
19. Cramer,J.M., Scarsdale,J.N., Walavalkar,N.M., Buchwald,W.A., Ginder,G.D. and Williams,D.C., Jr. (2014) Probing the dynamic distribution of bound states for methylcytosine-binding domains on DNA. *J. Biol. Chem.*, **289**, 1294–1302.
20. Shimbo,T., Du,Y., Grimm,S.A., Dhasarathy,A., Mav,D., Shah,R.R., Shi,H. and Wade,P.A. (2013) MBD3 localizes at promoters, gene bodies and enhancers of active genes. *PLoS Genet.*, **9**, e1004028.
21. Baubec,T., Ivanek,R., Lienert,F. and Schubeler,D. (2013) Methylation-dependent and -independent genomic targeting principles of the MBD protein family. *Cell*, **153**, 480–492.
22. Gunther,K., Rust,M., Leers,J., Boettger,T., Scharfe,M., Jarek,M., Bartkuhn,M. and Renkawitz,R. (2013) Differential roles for MBD2 and MBD3 at methylated CpG islands, active promoters and binding to exon sequences. *Nucleic Acids Res.*, **41**, 3010–3021.
23. Bhattacharya,S.K., Ramchandani,S., Cervoni,N. and Szyf,M. (1999) A mammalian protein with specific demethylase activity for mCpG DNA. *Nature*, **397**, 579–583.
24. Detich,N., Theberge,J. and Szyf,M. (2002) Promoter-specific activation and demethylation by MBD2/demethylase. *J. Biol. Chem.*, **277**, 35791–35794.
25. Brown,S.E. and Szyf,M. (2007) Epigenetic programming of the rRNA promoter by MBD3. *Mol. Cell. Biol.*, **27**, 4938–4952.
26. Brown,S.E., Suderman,M.J., Hallett,M. and Szyf,M. (2008) DNA demethylation induced by the methyl-CpG-binding domain protein MBD3. *Gene*, **420**, 99–106.
27. Tatematsu,K.I., Yamazaki,T. and Ishikawa,F. (2000) MBD2-MBD3 complex binds to hemi-methylated DNA and forms a complex containing DNMT1 at the replication foci in late S phase. *Genes Cells*, **5**, 677–688.
28. Cui,Y. and Irudayaraj,J. (2014) Inside single cells: quantitative analysis with advanced optics and nanomaterials. *Wiley Interdiscip. Rev. Nanomed. Nanobiotechnol.*, doi:10.1002/wnan.1321.
29. Miller,A., Chen,J., Takasuka,T.E., Jacobi,J.L., Kaufman,P.D., Irudayaraj,J.M. and Kirchmaier,A.L. (2010) Proliferating cell nuclear antigen (PCNA) is required for cell cycle-regulated silent chromatin on replicated and nonreplicated genes. *J. Biol. Chem.*, **285**, 35142–35154.
30. Chen,J., Miller,A., Kirchmaier,A.L. and Irudayaraj,J.M. (2012) Single-molecule tools elucidate H2A.Z nucleosome composition. *J. Cell Sci.*, **125**, 2954–2964.
31. Cui,Y., Cho,I.H., Chowdhury,B. and Irudayaraj,J. (2013) Real-time dynamics of methyl-CpG-binding domain protein 3 and its role in DNA demethylation by fluorescence correlation spectroscopy. *Epigenetics*, **8**, 1089–1100.
32. Slaughter,B.D., Schwartz,J.W. and Li,R. (2007) Mapping dynamic protein interactions in MAP kinase signaling using live-cell fluorescence fluctuation spectroscopy and imaging. *Proc. Natl. Acad. Sci. U.S.A.*, **104**, 20320–20325.
33. Chen,J. and Irudayaraj,J. (2009) Quantitative investigation of compartmentalized dynamics of ErbB2 targeting gold nanorods in live cells by single molecule spectroscopy. *ACS Nano*, **3**, 4071–4079.
34. Cui,Y., Choudhury,S.R. and Irudayaraj,J. (2014) Quantitative real-time kinetics of optogenetic proteins CRY2 and CIB1/N using single-molecule tools. *Anal. Biochem.*, **458**, 58–60.
35. Kapusta,P., Machan,R., Benda,A. and Hof,M. (2012) Fluorescence lifetime correlation spectroscopy (FLCS): concepts, applications and outlook. *Int. J. Mol. Sci.*, **13**, 12890–12910.
36. Machan,R., Kapusta,P. and Hof,M. (2014) Statistical filtering in fluorescence microscopy and fluorescence correlation spectroscopy. *Anal. Bioanal. Chem.*, **406**, 4797–4813.
37. Krude,T. (1999) Mimosine arrests proliferating human cells before onset of DNA replication in a dose-dependent manner. *Exp. Cell Res.*, **247**, 148–159.
38. Taniguchi,T., Garcia-Higuera,I., Andreassen,P.R., Gregory,R.C., Grompe,M. and D'Andrea,A.D. (2002) S-phase-specific interaction of the Fanconi anemia protein, FANCD2, with BRCA1 and RAD51. *Blood*, **100**, 2414–2420.
39. Al-Bader,A.A., Orengo,A. and Rao,P.N. (1978) G2 phase-specific proteins of HeLa cells. *Proc. Natl. Acad. Sci. U.S.A.*, **75**, 6064–6068.
40. Juan,G., Traganos,F. and Darzynkiewicz,Z. (2001) Methods to identify mitotic cells by flow cytometry. *Methods Cell Biol.*, **63**, 343–354.
41. Robertson,K.D., Keyomarsi,K., Gonzales,F.A., Velicescu,M. and Jones,P.A. (2000) Differential mRNA expression of the human DNA methyltransferases (DNMTs) 1, 3a and 3b during the G(0)/G(1) to S phase transition in normal and tumor cells. *Nucleic Acids Res.*, **28**, 2108–2113.
42. Woodcock,D.M., Simmons,D.L., Crowther,P.J., Cooper,I.A., Trainor,K.J. and Morley,A.A. (1986) Delayed DNA methylation is an integral feature of DNA-replication in mammalian-cells. *Exp. Cell Res.*, **166**, 103–112.
43. Enderlein,J. and Gregor,I. (2005) Using fluorescence lifetime for discriminating detector afterpulsing in fluorescence-correlation spectroscopy. *Rev. Sci. Instrum.*, **76**, doi:10.1063/1.1863399.
44. Chen,J., Nag,S., Vidi,P.A. and Irudayaraj,J. (2011) Single molecule in vivo analysis of toll-like receptor 9 and CpG DNA interaction. *PLoS One*, **6**, e17991.
45. Khrapunov,S., Warren,C., Cheng,H., Berko,E.R., Greally,J.M. and Brenowitz,M. (2014) Unusual characteristics of the DNA binding domain of epigenetic regulatory protein MeCP2 determine its binding specificity. *Biochemistry*, **53**, 3379–3391.
46. Feng,Q. and Zhang,Y. (2001) The MeCP1 complex represses transcription through preferential binding, remodeling, and deacetylating methylated nucleosomes. *Genes Dev.*, **15**, 827–832.
47. Jiang,C.L., Jin,S.G. and Pfeifer,G.P. (2004) MBD3L1 is a transcriptional repressor that interacts with methyl-CpG-binding protein 2 (MBD2) and components of the NuRD complex. *J. Biol. Chem.*, **279**, 52456–52464.
48. Kaji,K., Caballero,I.M., MacLeod,R., Nichols,J., Wilson,V.A. and Hendrich,B. (2006) The NuRD component Mbd3 is required for pluripotency of embryonic stem cells. *Nat. Cell Biol.*, **8**, 285–292.
49. Reynolds,N., Salmon-Divon,M., Dvinge,H., Hynes-Allen,A., Balasooriya,G., Leaford,D., Behrens,A., Bertone,P. and Hendrich,B. (2012) NuRD-mediated deacetylation of H3K27 facilitates recruitment of Polycomb Repressive Complex 2 to direct gene repression. *EMBO J.*, **31**, 593–605.

50. Noh,E.J., Lim,D.S. and Lee,J.S. (2009) A novel role for methyl CpG-binding domain protein 3, a component of the histone deacetylase complex, in regulation of cell cycle progression and cell death. *Biochem. Biophys. Res. Commun.*, **378**, 332–337.
51. Bibikova,M., Le,J., Barnes,B., Saedinia-Melnyk,S., Zhou,L.X., Shen,R. and Gunderson,K.L. (2009) Genome-wide DNA methylation profiling using Infinium (R) assay. *Epigenomics*, **1**, 177–200.
52. Knox,J.D., Araujo,F.D., Bigey,P., Slack,A.D., Price,G.B., Zannis-Hadjopoulos,M. and Szyf,M. (2000) Inhibition of DNA methyltransferase inhibits DNA replication. *J. Biol. Chem.*, **275**, 17986–17990.
53. Milutinovic,S., Zhuang,Q., Niveleau,A. and Szyf,M. (2003) Epigenomic stress response. Knockdown of DNA methyltransferase 1 triggers an intra-S-phase arrest of DNA replication and induction of stress response genes. *J. Biol. Chem.*, **278**, 14985–14995.
54. Yamaguchi,T., Cubizolles,F., Zhang,Y., Reichert,N., Kohler,H., Seiser,C. and Matthias,P. (2010) Histone deacetylases 1 and 2 act in concert to promote the G1-to-S progression. *Genes Dev.*, **24**, 455–469.
55. Ohki,I., Shimotake,N., Fujita,N., Jee,J.G., Ikegami,T., Nakao,M. and Shirakawa,M. (2001) Solution structure of the methyl-CpG binding domain of human MBD1 in complex with methylated DNA. *Cell*, **105**, 487–497.
56. Zou,X.Q., Ma,W., Solov'yov,I.A., Chipot,C. and Schulten,K. (2012) Recognition of methylated DNA through methyl-CpG binding domain proteins. *Nucleic Acids Res.*, **40**, 2747–2758.
57. Gnanapragasam,M.N., Scarsdale,J.N., Amaya,M.L., Webb,H.D., Desai,M.A., Walavalkar,N.M., Wang,S.Z., Zu Zhu,S., Ginder,G.D. and Williams,D.C. Jr (2011) p66Alpha-MBD2 coiled-coil interaction and recruitment of Mi-2 are critical for globin gene silencing by the MBD2-NuRD complex. *Proc. Natl. Acad. Sci. U.S.A.*, **108**, 7487–7492.
58. Steinmetz,M.O., Jelesarov,I., Matousek,W.M., Honnappa,S., Jahnke,W., Missimer,J.H., Frank,S., Alexandrescu,A.T. and Kammerer,R.A. (2007) Molecular basis of coiled-coil formation. *Proc. Natl. Acad. Sci. U.S.A.*, **104**, 7062–7067.
59. Walavalkar,N.M., Gordon,N. and Williams,D.C. (2013) Unique features of the anti-parallel, heterodimeric coiled-coil interaction between Methyl-cytosine Binding Domain 2 (MBD2) Homologues and GATA Zinc Finger Domain containing 2A (GATAD2A/p66 alpha). *J. Biol. Chem.*, **288**, 3419–3427.
60. Zhu,D., Fang,J., Li,Y. and Zhang,J. (2009) Mbd3, a component of NuRD/Mi-2 complex, helps maintain pluripotency of mouse embryonic stem cells by repressing trophectoderm differentiation. *PLoS One*, **4**, e7684.
61. Reynolds,N., Latos,P., Hynes-Allen,A., Loos,R., Leaford,D., O'Shaughnessy,A., Mosaku,O., Signolet,J., Brennecke,P., Kalkan,T. *et al.* (2012) NuRD suppresses pluripotency gene expression to promote transcriptional heterogeneity and lineage commitment. *Cell Stem Cell*, **10**, 583–594.
62. Pontes,T.B., Chen,E.S., Gigek,C.O., Calcagno,D.Q., Wisnieski,F., Leal,M.F., Demachki,S., Assumpcao,P.P., Artigiani,R., Lourenco,L.G. *et al.* (2014) Reduced mRNA expression levels of MBD2 and MBD3 in gastric carcinogenesis. *Tumour Biol.*, **35**, 3447–3453.
63. dos Santos,R.L., Tosti,L., Radzisheuskaya,A., Caballero,I.M., Kaji,K., Hendrich,B. and Silva,J.C.R. (2014) MBD3/NuRD facilitates induction of pluripotency in a context-dependent manner. *Cell Stem Cell*, **15**, 102–110.